

On the two-way interaction between homogeneous turbulence and dispersed solid particles. I: Turbulence modification

S. Elghobashi and G. C. Truesdell

Department of Mechanical and Aerospace Engineering, University of California, Irvine, California 92717

(Received 11 September 1992; accepted 29 March 1993)

The modification of decaying homogeneous turbulence due to its interaction with dispersed small solid particles ($d/\eta < 1$), at a volumetric loading ratio $\phi_v \leq 5 \times 10^{-4}$, is studied using direct numerical simulation. The results show that the particles increase the fluid turbulence energy at high wave numbers. This increase of energy is accompanied by an increase of the viscous dissipation rate, and, hence, an increase in the rate of energy transfer $T(k)$ from the large-scale motion. Thus, depending on the conditions at particle injection, the fluid turbulence kinetic energy may increase initially. But, in the absence of external sources (shear or buoyancy), the turbulence energy eventually decays faster than in the particle-free turbulence. In gravitational environment, particles transfer their momentum to the small-scale motion but in an *anisotropic* manner. The pressure-strain correlation acts to remove this anisotropy by transferring energy from the direction of gravity to the other two directions, *but at the same wave number*, i.e., to the small-scale motion in directions normal to gravity. This input of energy in the two directions with lowest energy content causes a *reverse cascade*. This reverse cascade tends to build up the energy level at lower wave numbers, thus reducing the decay rate of energy as compared to that of either the particle-free turbulence or the zero-gravity particle-laden flow.

I. INTRODUCTION

It has been known for more than three decades that the addition of solid or liquid particles, at volume fraction as low as 10^{-5} , to a turbulent flow modifies the structure of turbulence, thus altering the transport rates of momentum and mass. This modification, in turn, affects particle dispersion, hence the two-way interaction. Available experimental data show that the addition of particles may *increase or decrease* the turbulence kinetic energy of the carrier fluid. However, there is a lack of understanding of the mechanisms responsible for this increase or decrease.

The few experimental data on particle-laden turbulent flows are valid only for the conditions of the experiment and cannot be generalized. In some experiments, the injection of fine droplets or solid particles (diameter $d < 250\mu$) into a free turbulent jet reduces the turbulence intensity, thus lowering the spreading rate of the half-width of the jet.¹⁻⁵ However, other experiments⁶ show that the addition of large particles ($d > 500\mu$) increases the turbulence intensity in a free jet, whereas smaller particles ($d < 250\mu$) suppress turbulence in the jet. Recently, Hardalupas *et al.*⁷ measured the velocities of the particles and fluid in turbulent particle-laden jets. They showed that the rate of spread of the half width of the jet increased with increasing the volume fraction of 80μ glass beads, whereas it decreased with increasing the volume fraction of 40μ beads. Hetsroni⁸ suggested that particles with low Reynolds number, R_p , cause turbulence suppression, while particles with higher Reynolds number enhance turbulence due to wake shedding. However, as will be shown later, the present study indicates that particles with low-Reynolds number, $R_p < 1$, can also increase the turbulence energy.

Gore and Crowe⁹ reviewed the available experimental data on turbulence modulation in particle-laden flows and

proposed that the critical parameter that predicts whether the turbulence will be augmented or suppressed with the addition of particles is d/l , where d is the particle diameter and l is the Eulerian integral length scale of turbulence. They concluded that the critical value is $d/l \approx 0.1$, above which turbulence intensity is increased and below which it is suppressed. While it is interesting to attempt to describe the effect of dispersed particles on turbulence via a single parameter, the study⁹ leaves the fundamental questions unanswered. For example, in that study,⁹ the augmentation of turbulence energy by the particles is attributed to the presence of their wakes. However, experimental evidence indicates that particles without wakes (small R_p) may also increase the turbulence energy.⁷ Furthermore, in highly anisotropic flows (e.g., in the neighborhood of solid walls) the length scale l depends strongly on the direction relative to the wall, and thus the parameter d/l would have *different values at the same location*. In addition, our present results show that turbulence intensity increases for $d/l \approx 10^{-3}$, thus contradicting the proposal of Gore and Crowe.

The purpose of this paper is to examine in some detail the two-way interaction between the particles and turbulence in a much simpler flow than the inhomogeneous flows reviewed above. In particular, the paper is concerned with the physics of interaction between a decaying homogeneous isotropic turbulence (or simply grid turbulence) and a large number of solid spherical particles dispersed within. We aim to answer the questions of how and why the turbulence modification takes place. Grid turbulence was selected for the study because of its spatial homogeneity and the independence of its properties on the mean flow velocity. We use the method of direct numerical simulation to solve the three-dimensional, time-dependent Navier-Stokes equations which include all the forces exerted by the

particles on the fluid. The volume fraction of the particles is large enough to modulate the turbulence, but small enough to avoid collisions between the particles. We examine the effects of the particles on the time development of turbulence energy and dissipation and their spatial spectra. Discussion of the effects of the modified turbulence on the dispersion of particles and the various Lagrangian statistics is the subject of another paper.¹⁰

Only one other direct numerical simulation study¹¹ has been reported concerning the two-way interaction of particles with homogeneous turbulence. However, that study considered only stationary turbulence by forcing the flow at the low wave numbers. Stationarity of turbulence was achieved by the addition of energy, at each time step, at a rate equal to that of the energy dissipation. Clearly, the results obtained from a forced simulation are questionable when the goal is to quantify the changes in the fluid turbulence energy spectrum caused by the particles. As will be discussed later in Sec. III, the addition of particles may increase or decrease the turbulence energy, a result that cannot be obtained from a stationary turbulence simulation. Furthermore, the particle motion equation used in that study¹¹ included only the drag force. The present study shows that neglecting the effects of gravity on particle motion results in a significantly different behavior of the turbulence in the carrier fluid.

II. MATHEMATICAL DESCRIPTION

The exact time-dependent, three-dimensional Navier–Stokes and continuity equations are solved in a cubical domain with periodic boundary conditions. Gravity acts downward in the negative x_3 direction. The two other coordinates x_1 and x_2 are in the horizontal plane. The fluid is incompressible and has a constant kinematic viscosity, ν . The dimensionless governing equations are

$$\frac{\partial u_i}{\partial t} + \frac{\partial}{\partial x_j} (u_j u_i) = \frac{1}{\text{Re}} \frac{\partial^2 u_i}{\partial x_j^2} - \frac{\partial p}{\partial x_i} - f_i, \quad (1)$$

$$\frac{\partial u_j}{\partial x_j} = 0. \quad (2)$$

The last term in Eq. (1) is the force, in the x_i direction, exerted per unit mass of fluid by N particles and calculated from

$$f_i = \sum_{n=1}^N f_{n,i}, \quad (3)$$

where $f_{n,i}$ is the instantaneous local sum, in the x_i direction, of the first four forces on the right-hand side (rhs) of Eq. (5) below acting on one particle n . Nondimensionalization of f_i is consistent with that of other terms in Eq. (1). Also, N is the instantaneous number of particles, $[N = N(x_1, x_2, x_3, t)]$, within the control volume at which Eq. (1) is integrated. When we study the dispersion of particles without effects on the fluid (i.e., one-way coupling or equivalently particle-free flow) we set f_i equal to zero. The direct effect of the particles presence on the continuity

equation of the fluid, Eq. (2), is assumed negligible since the volume fraction of the particles in our study is less than 10^{-3} .

The equations are discretized in an Eulerian framework using a second-order finite-difference technique on a staggered grid containing 96^3 points. This grid permits an initial microscale Reynolds number $R_{\lambda,0} = 35$. The Adams–Bashforth scheme is used to integrate the equations in time. Pressure is treated implicitly, and is obtained by solving the Poisson equation in finite-difference form using a fast Poisson solver. More details about the numerical method and its accuracy are discussed by Elghobashi and Truesdell¹² and Gerz *et al.*¹³

The initialization algorithm insures, for a prescribed energy spectrum, that the initial random velocity field is isotropic, periodic in the three spatial directions, and divergence free with respect to the discretized form of the continuity equation. It also ensures that the velocity cross-correlation spectra, $R_{ij}(k)$, satisfy the realizability constraints.¹⁴

The energy spectrum $E(k,0)$ at dimensionless time $T=0$ is prescribed by

$$E(k,0) = \left(\frac{3u_0^2}{2}\right) \left(\frac{1}{2\pi}\right) \left(\frac{k}{k_p}\right) \exp\left(\frac{-k}{k_p}\right), \quad (4)$$

where u_0 is the dimensionless rms velocity, k is the wave number, and k_p is the wave number of peak energy. All the wave numbers appearing in Eq. (4) are normalized by the lowest nonzero wave number, k_{\min} , which equals 2π since the size of the computational domain $L=1$. The two inputs u_0 and k_p are sufficient to specify $E(k,0)$. The dimensionless kinematic viscosity ν is calculated from the prescribed initial microscale Reynolds number, $R_{\lambda,0}$, and the computed initial energy dissipation rate ϵ_0 . The values of the dimensionless parameters used in the present simulation at $T=0$ are $R_{\lambda,0} = 35$, $(k_p/k_{\min})=4$, $u_0=0.0508$, $\lambda_0=0.0348$, $\epsilon_0=0.00162$, $\nu=5.05 \times 10^{-5}$. The initial integral length scale $l_0=0.0715$ and Kolmogorov length scale $\eta_0=0.0029$. The values of the reference length and time scales used in normalizing these quantities are, respectively, $L_{\text{ref}}=0.1859$ m and $T_{\text{ref}}=0.1068$ sec.

The ability of the simulation to resolve the motion at the smallest turbulence scales is measured by the dimensionless quantity ηk_{\max} , where k_{\max} is the highest resolved wave number $[=2\pi(N_g/2)]$. Here, N_g is the number of grid points in each coordinate direction ($N_g=96$). In our simulations $1 < \eta k_{\max} < 1.7$ for $0.75 < T < 6$.

The solid particles are added to the flow at time $T=0.75$ when the magnitude of the skewness of the velocity derivative reaches about 0.47, indicating an established rate of energy transfer across the energy spectrum.

The instantaneous velocity of each particle, v_i , in the x_i direction, is obtained by time integration of the Lagrangian equation of particle motion:

$$\begin{aligned}
m_p \left(\frac{dv_i}{dt_p} \right) &= \frac{m_p(u_i - v_i)}{\tau_p} + m_f \left(\frac{Du_i}{Dt} \right) + \frac{1}{2} m_f \left(\frac{Du_i}{Dt} - \frac{dv_i}{dt_p} \right) \\
&+ 6a^2 (\pi \rho \mu)^{1/2} \int_{t_{p0}}^{t_p} \frac{d/d\tau (u_i - v_i)}{(t_p - \tau)^{1/2}} d\tau \\
&+ (m_p - m_f) g_i. \tag{5}
\end{aligned}$$

Equation (5) describes the balance of forces acting on the particle as it moves along its trajectory. The term on the left-hand side (lhs) is the inertia force acting on the particle due to its acceleration. The terms on the right side are, respectively, the forces due to viscous and pressure drag, fluid pressure gradient and viscous stresses, inertia of virtual mass, viscous drag due to unsteady relative acceleration (Basset), and buoyancy. The response time, τ_p , is the time for momentum transfer due to drag and is calculated from

$$\frac{1}{\tau_p} = \left(\frac{3}{8a} \right) C_D \left(\frac{\rho}{\rho_p} \right) |u_i - v_i|. \tag{6}$$

The quantities a , m_p , ρ_p are, respectively, the particle radius, mass and material density. Here, C_D is the total drag coefficient, which is assumed a function of the Reynolds number of the particle, $R_p = 2a\rho|u_i - v_i|/\mu$. The fluid density and viscosity are ρ and μ . The derivative d/dt_p is, with respect to time, following the moving particle, whereas Du_i/Dt is the total acceleration of the fluid as seen by the particle, $Du_i/Dt = [(\partial u_i/\partial t) + u_j(\partial u_i/\partial x_j)]$, evaluated at the particle position \mathbf{x}_p . It should be pointed out that Eq. (5) is strictly valid for an *isolated particle*, where there are no effects of other particles on either the fluid or the particle of interest. In particular, the derivation of the term (Du_i/Dt) , which accounts for the force on the particle due to the fluid pressure gradient and viscous stresses, was based on the assumption that there is no two-way coupling. However, the computed magnitude of this term is of the order of 10^{-3} times that of the drag term and thus has negligible effect on the present results. In fact, there is no known exact Lagrangian equation that governs the motion of a particle in a turbulent flow with *two-way coupling*. The only alternative at present is to solve numerically the Navier–Stokes equations around individual particles. For example, a recent study¹⁵ examines the laminar flow around two neighboring particles. Details of integrating Eq. (5) to obtain the instantaneous particle velocity and position are given by Elghobashi and Truesdell.¹² In addition to insuring the resolution of the small scale motion as discussed earlier ($\eta k_{\max} > 1$), it is necessary that the instantaneous fluid velocity $u_i(\mathbf{x}_p, t)$ at the location of the particle be accurately calculated. We compute this velocity via a fourth-order accurate, two-dimensional, four-point Hermitian cubic polynomial interpolation scheme between the adjacent Eulerian fluid velocity values. This scheme is applied in the three coordinate directions at the particle location. We have compared the accuracy of this scheme with 12 others including linear interpolation, Lagrange with 36 points, midpoint with 21 points, midplane with 24 points, and third-order Taylor series with 13 points.¹⁶ It

TABLE I. Particle properties for the study of the effects of τ_p^* .

Case	τ_p^*	d	ρ_p/ρ	ϕ_v	ϕ_m
A	0.0	0.0
B	0.25	5.0×10^{-4}	909	2.5×10^{-4}	0.23
C	0.50	5.0×10^{-4}	1818	2.5×10^{-4}	0.45
D	1.00	5.0×10^{-4}	3636	2.5×10^{-4}	0.91

was concluded that the fourth-order accurate Hermitian scheme is superior to the other schemes regarding the combination of accuracy and computational economy. Balachandar and Maxey¹⁷ used a fourth-order Hermitian scheme in two directions followed by a Fourier interpolation in the third direction. The accuracy of our scheme compares well with theirs. Furthermore, the number of computational particles should be large enough to obtain an ensemble average of the independent realizations of the random dispersion process. Truesdell¹⁸ investigated the effect of the ratio of the number of actual (for a given ϕ_v) to computational particles on the time development of all the statistical quantities presented here and concluded that one computational particle representing 100 actual particles provides results within 2% of those obtained with half this number. A typical simulation requires about 65 CPU hours on the Convex C-240 computer or about 35 CPU h on the Cray-Y-MP8/864.

III. RESULTS

A. Effects of particles inertia

We study the modification of turbulence due to the two-way interaction between the fluid and particles by varying particles inertia in the absence of gravity. We vary three parameters, the particle response time, τ_p , the particle diameter, d , and the volumetric fraction, ϕ_v , one at a time, to examine their effects.

1. Effects of particle response time

Here, we compare the results of three two-way coupling cases (B, C, and D) with those of case A in which the particles are not allowed to influence the fluid motion [$f_i=0$ in Eq. (1)]. The particle properties are listed in Table I. The particles in the three cases have the same volumetric fraction, ϕ_v , and diameter d , but different particle response time at injection, τ_p^* . All quantities in this and other tables throughout the paper are dimensionless via normalization by L_{ref} and T_{ref} unless stated otherwise. We increase τ_p^* from 0.25 for case B by factors of 2 and 4 for cases C and D, respectively. This is achieved by increasing the particle material density, ρ_p , in C and D, by the same factors, relative to that of B. The mass loading ratio, ϕ_m , increases accordingly. The fluid density, ρ , is kept constant ($=1 \text{ kg/m}^3$) throughout. Table II lists the particle properties normalized by the relevant turbulence length or time scale. The first two columns contain the time-scale ratios τ_p^*/τ_f and τ_p^*/τ_K , where the value to the left of \Rightarrow is at the time of particle injection ($T=0.75$), and that to the

TABLE II. Particle properties normalized by relevant scales of turbulence.

Case	τ_p^*/τ_f	τ_p^*/τ_K	d/l^*	d/η^*	$R_{p,max}$
B	0.144 \Rightarrow 0.043	1.263 \Rightarrow 0.391	0.007	0.158	0.18
C	0.289 \Rightarrow 0.079	2.252 \Rightarrow 0.764	0.007	0.158	0.27
D	0.578 \Rightarrow 0.129	5.051 \Rightarrow 1.510	0.007	0.158	0.36

right is at the end of the simulation ($T=6$). The turnover time of the large eddies is $\tau_f=l/u_{rms}$, and the Kolmogorov time scale is $\tau_K=(\nu/\epsilon)^{1/2}$, where

$$l(t) = \frac{1}{2u_{rms}^2(t)} \int \frac{E(k,t)}{k} dk, \quad (7)$$

and

$$\epsilon(t) = 2\nu \int k^2 E(k,t) dk. \quad (8)$$

It is seen that the two ratios decrease with time due to the increase of the time scales of the decaying turbulence. The time $T=6$ is about 4.3 times the initial eddy turnover time, $\tau_{f,0}$. Continuing the simulation of case D beyond this time may result in lowering the value of R_λ below 14 and, hence, weak turbulence. The values of R_λ at $T=6$ for cases A, B, and C are, respectively, 19.5, 18, and 16.5. The third and fourth columns list the particle diameter, normalized by the integral length scale, l^* , and the Kolmogorov scale, η^* , at the time of particle injection. Also listed is the maximum value of the particle Reynolds number, $R_{p,max}$, which is seen to be less than 0.4 throughout the simulations. Figure 1 shows the time development of the turbulence kinetic energy $E(t)$, normalized by its initial value, for cases A, B, C, and D. The particles are injected, at dimensionless time $T=0.75$, with their instantaneous velocity equal to that of their surrounding fluid, thus the four curves coincide up to a time $T \approx 1.5$ after which the two-way coupling effects start to be noticeable. In case A, the particles do not influ-

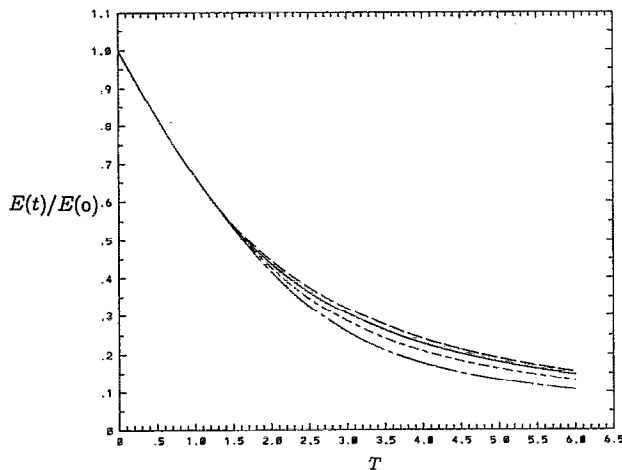


FIG. 1. Effect of varying τ_p (Table I) on the time development of turbulence kinetic energy $E(t)$ normalized by its initial value $E(0)$ for case A: ---, B: —, C: - · - · -, D: - - -.

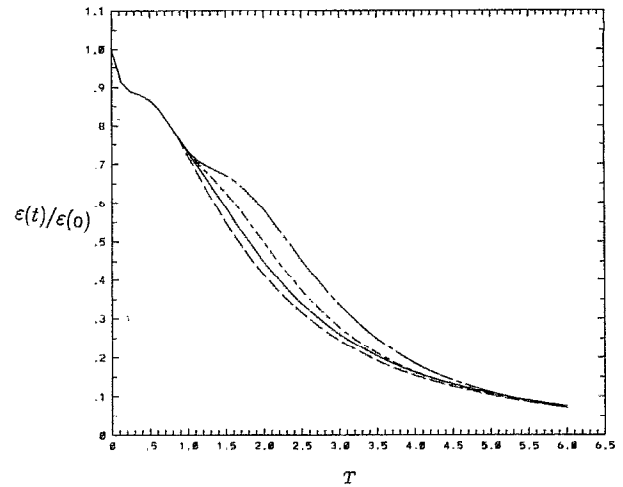


FIG. 2. Effect of varying τ_p (Table I) on the time development of the dissipation rate of turbulence kinetic energy $\epsilon(t)$ normalized by its initial value $\epsilon(0)$ for case A: ---, B: —, C: - · - · -, D: - - -.

ence the flow, and thus the dashed curve A follows the standard decay rate of grid turbulence. It is seen that the higher τ_p^* the lower is the value of $E(t)$. This is also evidenced in Fig. 2 by the corresponding increase with τ_p^* of the energy dissipation rate $\epsilon(t)$ shown normalized by its initial value for the same cases. In order to examine whether the reduction of $E(t)$ and the augmentation of $\epsilon(t)$ are uniformly or preferentially distributed over the scales of turbulence we display the three-dimensional energy and dissipation spectra $E(k,t)$ and $D(k,t)$ of the four cases at time $T=4$ in Figs. 3 and 4. It is seen that for k larger than about 18 the values of both $E(k)$ and $D(k)$ for B, C, and D exceed those of A, and for $k < 18$ the values for B, C, and D are less than that of A. Also, the higher τ_p^* the larger is the deviation from A. The behavior of $E(k)$ and $D(k)$ displayed in Figs. 3 and 4, i.e., the crossover at $k \approx 18$, is typical throughout our simulation. Now, since the values of $E(t)$ for B, C, and D are lower than that of A (Fig. 1), it is obvious that the reduction of $E(k)$ in the low wave-number range ($k < 18$) outweighs its increase at higher wave numbers since $E(t) = \int_0^\infty E(k,t) dk$. On the other hand, the augmentation of $\epsilon(t)$ for B, C, and D (Fig. 2) is mainly due to the enhancement by the particles of $D(k,t)$ in the high wave-number range ($k > 18$).

It is clear that the modulation of $E(k,t)$ and $D(k,t)$ by the particles follows a pattern of *selective spectral redistribution* rather than a *uniform attenuation or augmentation* over the entire spectrum. Since the particles are small ($d < \eta$ and $\tau_p \approx \tau_K$) it is expected, at least intuitively, that they act as randomly distributed disturbances within the small-scale (high wave number) motion, providing a source (or sink) of energy proportional to the correlation $\langle u_i f_i \rangle$, where $\langle \rangle$ denotes ensemble averaging. It is straightforward to show, by starting from Eq. (1), that this correlation appears as a source (sink) in the transport equation of the kinetic energy of turbulence in the physical space.

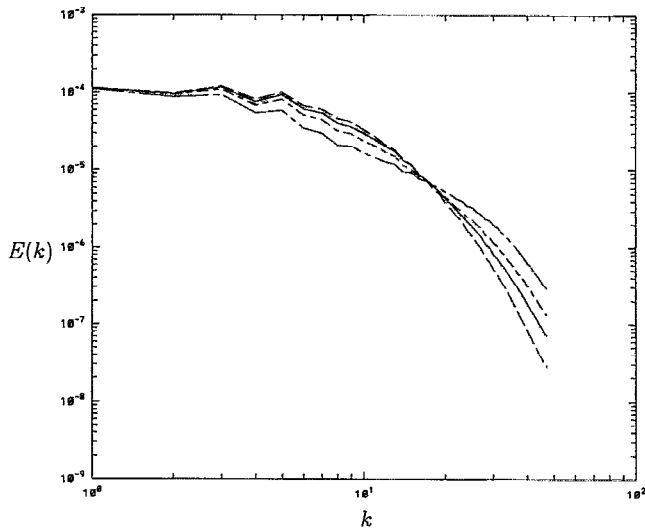


FIG. 3. Effect of varying τ_p (Table I) on the three-dimensional spatial spectrum of energy $E(k)$ at time $T=4$ for case A: ---, B: —, C: - · - · -, D: - - -.

Now, since it is not expected that the small particles influence the large-scale (small wave number) motion *directly*, we need to understand the mechanisms leading to the modulation of $E(k,t)$ and $D(k,t)$ at small values of k (Figs. 3 and 4). Thus it is instructive to examine the spectral distribution of $T(k,t)$, the rate of energy transfer to wave numbers of magnitude k . In particle-free homogeneous turbulence, the time rate of change of energy $E(k,t)$ at wave number k is related to the net rate of energy transfer $T(k,t)$ (Batchelor¹⁹) according to

$$\frac{dE(k,t)}{dt} = T(k,t) - D(k,t), \quad (9)$$

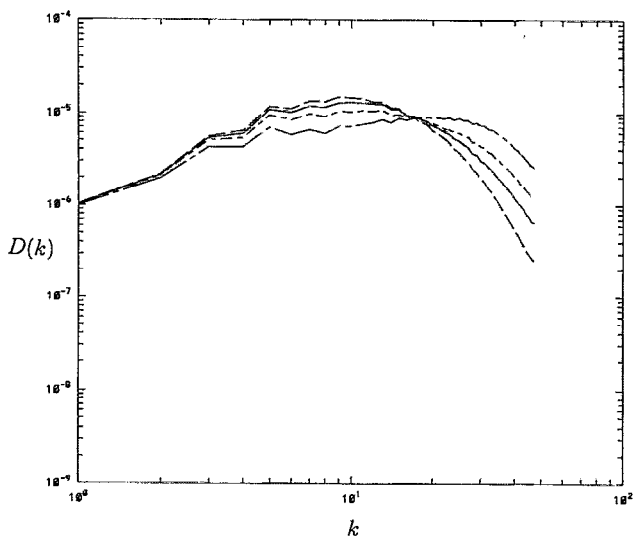


FIG. 4. Effect of varying τ_p (Table I) on the three-dimensional spatial spectrum of energy dissipation $D(k)$ at time $T=4$ for case A: ---, B: —, C: - · - · -, D: - - -.

where the viscous dissipation rate $D(k,t) = 2\nu k^2 E(k,t)$. Also, the total spectral flux of energy from wave number k to all higher wave numbers is

$$F(k,t) = \int_k^\infty T(k',t) dk', \quad (10)$$

and thus

$$-F(k,t) = \int_0^k T(k',t) dk'. \quad (11)$$

Explicit reference to the time dependence of $E(k,t)$, $D(k,t)$, and $T(k,t)$ will be omitted hereinafter for convenience. Mathematically, $T(k)$ originates from the nonlinear (inertia) terms of the Navier–Stokes equation in the Fourier space. Detailed derivation of (9) from the transport equation of the two-velocity two-point correlation is given by Hinze.²⁰ The multiplication of two-velocity Fourier components with wave numbers q and $(k-q)$ forms a component with wave number k , i.e., the three wave vectors form a triad with zero sum. Thus $T(k)$ represents an integrated effect of the interactions of all triads with one leg fixed as k , the second leg is any other wave number in the spectrum, and the third satisfies the condition of vanishing sum of the three wave vectors. This means that the nonlinear inertia force transports $E(k)$ between different wave numbers for the same velocity component. The need to understand the physics of *local* (when the ratio of two wave numbers, or legs, in the triad does not exceed 2) and *nonlocal* triadic interactions in homogeneous isotropic turbulence resulted in a number of recent studies.^{21–23} We compute $T(k)$ from the Fourier transform of the two-point third-order velocity-correlation tensor $\langle u_i(x)u_j(x)u_l(x+r) \rangle$ following the procedure outlined by Van Atta and Chen.²⁴

Now, in particle-laden turbulence with two-way coupling, the derivation of Eq. (9) from the Fourier transform of the transport equation of the two-velocity two-point correlation results in additional terms originating from the correlation $\langle u_i f_i \rangle$. As was mentioned earlier, we compute f_i from the sum of the forces exerted by the particles on the fluid. However, since the drag force dominates the other forces¹² contributing to f_i , and only to facilitate the discussion we assume here that $\langle u_i f_i \rangle \approx \langle \Phi_p u_i (v_i - u_i) / \tau_p \rangle$, where Φ_p is the local volume fraction of the particles. We denote the Fourier transform of this second-order correlation as $\Psi_p(k)$ which represents a local source or sink of energy depending on the sign of the correlation in the physical space, thus modifying $E(k)$, $D(k)$, and $T(k)$. Accordingly, Eq. (9) becomes

$$\frac{dE(k)}{dt} = T(k) - 2\nu k^2 E(k) + \Psi_p(k). \quad (12)$$

It is seen from Eq. (12) that $T(k)$ is the only term that affects $dE(k)/dt$ at small k *directly* due to disturbances at much higher wave numbers, i.e., due to *nonlocal* triadic interactions. Figure 5 displays the computed $T(k_1)$, the component of $T(k)$ in the x_1 direction, for cases A and D at time $T=2$. The other two components, $T(k_2)$ and $T(k_3)$, are nearly identical to $T(k_1)$, as expected in iso-

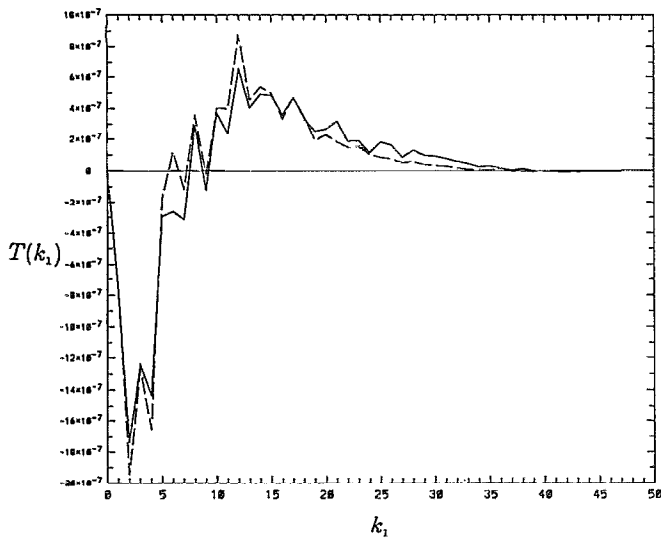


FIG. 5. Effect of varying τ_p (Table I) on the spectral distribution of $T(k_1)$ at time $T=2$ for case A: ---, D: —.

tropic turbulence, and thus are not shown here. It is noted that $T(k_1)$ vanishes at $k \approx 40$, i.e., well below the maximum value of k in our simulation ($=48$), indicating sufficient resolution of the motion at the smallest scales. The shape of $T(k_1)$ for case A, the dashed line, is as expected for homogeneous turbulence.^{22,24} The effects of the two-way coupling are manifested in the positive transfer region ($k_1 > 8$) by the increase of $T(k_1)$ of case D (solid line) relative to that of A for $k_1 > 18$ and its reduction relative to A for $k_1 < 18$. A similar behavior is seen in the negative transfer region, with an increase in the magnitude of $T(k_1)$ of D relative to A for $6 < k_1 < 8$, and its reduction for $2 < k_1 < 5$. As was mentioned earlier in the discussion of Figs. 3 and 4, both $E(k)$ and $D(k)$ displayed a crossover behavior for cases B, C, and D relative to A at $k \approx 18$, the same crossover wave number of $T(k_1)$ in Fig. 5.

In order to examine further the effects of the two-way coupling on both $T(k)$ and $D(k)$ we display the time distribution of the skewness, $S(t)$, of the velocity derivative for cases A, B, C, and D in Fig. 6. The skewness $S(t)$ is defined as

$$S(t) \equiv -\frac{1}{3} \sum_{i=1}^3 \left\langle \left(\frac{\partial u_i}{\partial x_i} \right)^3 \right\rangle / \left(\frac{1}{3} \sum_{i=1}^3 \left\langle \left(\frac{\partial u_i}{\partial x_i} \right)^2 \right\rangle \right)^{3/2}, \quad (13)$$

and is related to $D(k)$ and $T(k)$, according to²⁵

$$S(t) = \left(\frac{3\sqrt{30}}{14} \right) \left(\int_0^\infty k^2 T(k,t) dk \right) / \left(\int_0^\infty k^2 E(k,t) dk \right)^{3/2}. \quad (14)$$

Thus the skewness is proportional to the ratio of $T(k)$ in the high wave-number range to $D^{3/2}(k)$ in that range. Figure 6 shows that the larger τ_p the smaller is $S(t)$. In order to see whether the reduction of $S(t)$ is mainly due to the 3/2 exponent of $D(k)$, or that the increase of $D(k)$ is

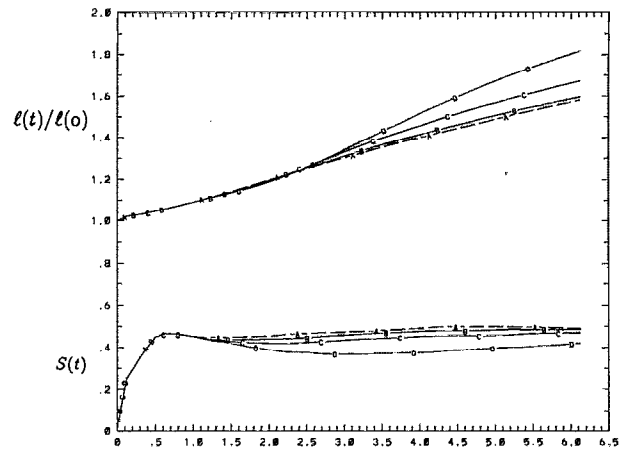


FIG. 6. Effect of varying τ_p (Table I) on the time development of the skewness of the fluid velocity derivative $S(t)$ for case A: ---, B: —, C: - · - · -, D: - - - and the integral length scale $l(t)$ normalized by its initial value, $l(0)$ for case A: ---, B: —, C: - · - · -, D: - - -.

higher than that of $T(k)$, we found that the latter is the case. The increase of $\int_0^\infty k^2 E(k,t) dk$ of cases B, C, and D relative to A is about 10% to 30% higher than the relative increase of $T(k)$, the larger difference being for case D. Also shown in Fig. 6 is the time development of the integral length scale $l(t)$ [see Eq. (8)]. It is seen that the larger τ_p the higher is the rate of growth of l . This indicates that the augmentation of $\epsilon(t)$ (Fig. 2) by the particles causes u_{rms}^2 , or the total energy, to decay at a rate faster than that of $E(k)$ of the smallest wave numbers [see Eq. (8) and Fig. 3]. In particular, the energy of the intermediate wave numbers ($5 < k < 15$) (Fig. 3) decays faster than that of $k < 5$. On the other hand, the larger τ_p the smaller is λ , as seen from

$$\lambda(t) = [15\nu u_{rms}^2(t)/\epsilon(t)]^{1/2}, \quad (15)$$

since the particles reduce u_{rms}^2 and increase ϵ simultaneously. Similarly, the particles reduce the Kolmogorov scale, $\eta(t) = [\nu^3/\epsilon(t)]^{1/4}$, as they augment ϵ .

Thus the physical picture that emerges from the above analysis is that the particles, due to their inertia and being smaller than the Kolmogorov length scale, impart their energy to the turbulent motion at high wave numbers (Fig. 3) with a corresponding increase in the dissipation (Fig. 4). This enhanced dissipation signals the smaller wave numbers (larger scales), via the nonlocal triadic interactions of $T(k)$ (Fig. 5), to supply more energy to the highly active small scales, at a rate higher than that of the particle-free case A. This results in the reduction of $E(k)$ of the energy-containing small-wave-number motion.

Figure 7 shows the time distribution of the correlation $\langle u_1(v_1 - u_1)/\tau_p \rangle$ for cases B, C, and D. As mentioned earlier, the velocity of the particles at injection is equal to that of their surrounding fluid. Thus, for a small time period thereafter, the correlation is positive and provides a source of energy, though not substantial, to the decaying turbulence. It is interesting to note that in all three cases, the particle diameter is much smaller than the integral length

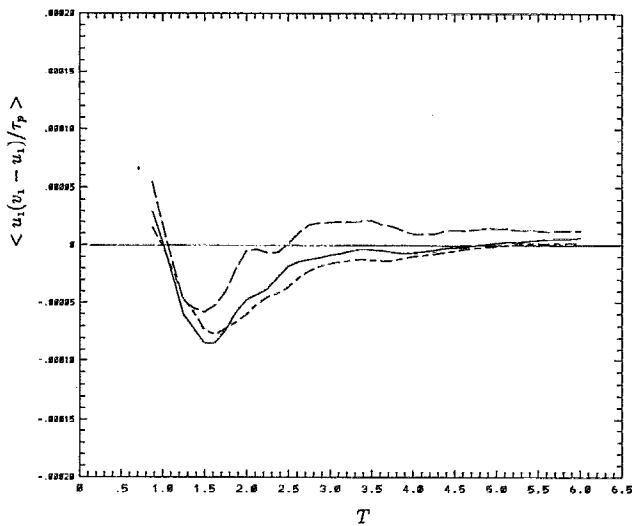


FIG. 7. Effect of varying τ_p (Table I) on the time development of the correlation $\langle u_1(v_1 - u_1)/\tau_p \rangle$ for case B: ---, C: —, D: - · - ·.

scale [$d/l^* = 0.007$ (Table II)], yet they provide a source of energy during the time $T < 1$. Had they been injected at a velocity larger than that of the surrounding fluid, the magnitude of that source would have been even greater and with longer lasting effects. This finding contrasts the suggestion of Gore and Crowe⁹ that the critical value is $d/l \approx 0.1$.

For $T > 1$, the crossing trajectories effect, due to the inertia of the particles, tends to decorrelate the velocities of particles and fluid and thus reduce the magnitude of $\langle u_1 v_1 \rangle$. The result is a negative $\langle u_1(v_1 - u_1)/\tau_p \rangle$, as seen in Fig. 7. In fact, the effect of the decorrelation (large negative numerator) outweighs the effect of the relative magnitude of τ_p among B, C, and D, as shown. As time in-

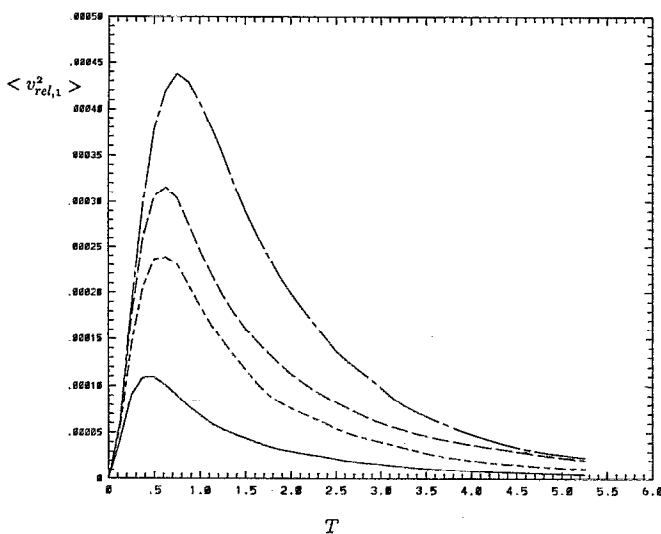


FIG. 8. Effect of varying τ_p (Table I) on the time development of mean-square relative velocity in the lateral direction x_1 of the particles for case A: ---, B: —, C: - · - ·, D: - · - · - ·.

TABLE III. Particle properties for the study of the effects of particle diameter.

Case	τ_p^*	d	ρ_p/ρ	ϕ_v	ϕ_m
C	0.50	5.0×10^{-4}	1818	2.5×10^{-4}	0.45
E	0.50	7.5×10^{-4}	808	2.5×10^{-4}	0.20
F	0.50	1.0×10^{-3}	455	2.5×10^{-4}	0.11

creases, the magnitude of the correlation diminishes because of the decay of the relative velocity of the particles, as seen in Fig. 8, which displays the time development of $\langle v_{rel,1}^2 \rangle = \langle (v_1 - u_1)^2 \rangle$ for the four cases. It should be noted that the time $T=0$ in Fig. 8 is the time of particle injection. The particles with the smallest τ_p , case B, have the smallest relative velocity as expected, and thus for $T > 2.5$ we see (in Fig. 7) a positive $\langle u_1 v_1 \rangle$ whose magnitude is greater than the energy component $\langle u_1 u_1 \rangle$ of the decaying turbulence. Case D, with the largest τ_p , experiences the highest relative velocity fluctuations. The dashed curve, A, in Fig. 8 is for particles identical to those in case C but without effect on the fluid. Comparing the curves A and C indicates clearly that two-way coupling reduces the relative velocity fluctuations, hence decreases R_p and increases the dissipation of energy.

2. Effects of particle diameter

The objective here is to examine the effects on the turbulence properties of varying the particle diameter while fixing the volumetric loading and the response time. This is equivalent to examining the effects of varying the total surface area of the particles by fixing their response time and total volumetric fraction but changing their number. Table III lists the properties of the particles in cases C, E, and F. The diameters in E and F are, respectively, 1.5 and 2 times that of C. This is achieved by reducing the particle material density, ρ_p , in E and F, by the square of these factors, relative to that of C, thus keeping τ_p^* the same. The mass loading ratio, ϕ_m , decreases accordingly. Table IV lists the particle properties normalized by the relevant turbulence length or time scale. It should be emphasized that the range of diameter variation is limited by two considerations. First, if the diameter is reduced considerably below that of case C, the number of particles increases and the costs of computer memory and CPU increase accordingly. For example, a reduction of the diameter by a factor of 2 increases the number of particles by a factor of 8. Second, we should insure that $d < \eta$ (Table IV) throughout the simulation in order to remain within the limits of validity of Eq. (5). Figure 9 displays the time development of $E(t)$ of cases A, C, E, and F. Doubling the

TABLE IV. Particle properties normalized by relevant scales of turbulence.

Case	τ_p^*/τ_f	τ_p^*/τ_K	d/l^*	d/η^*	$R_{p,max}$
E	$0.289 \Rightarrow 0.083$	$2.525 \Rightarrow 0.780$	0.010	0.237	0.35
F	$0.289 \Rightarrow 0.085$	$2.525 \Rightarrow 0.770$	0.013	0.316	0.45

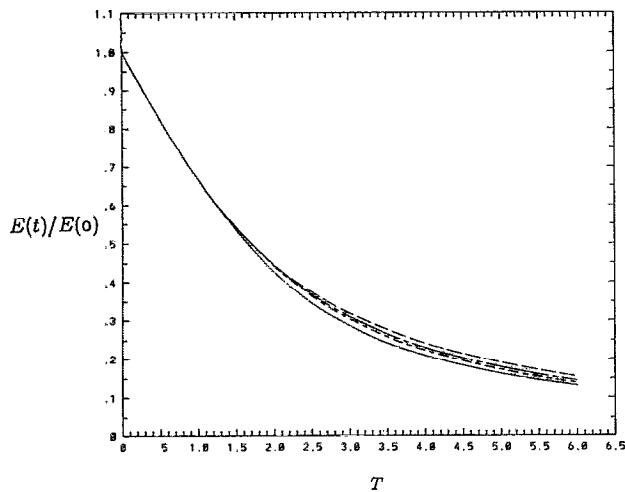


FIG. 9. Effect of varying particle diameter (Table III) on the time development of turbulence kinetic energy $E(t)$ normalized by its initial value $E(0)$ for case A: ---, C: —, E: - · - ·, F: - - -.

particle diameter (case F relative to C) while fixing the volumetric fraction, reduces the number of particles by a factor of 8 and the total surface area by a factor of 2, and hence reduces the two-way coupling effects. It is clear from the figure, as expected, that doubling the particle diameter, while fixing τ_p and ϕ_v has insignificant effects on the turbulence, as compared to doubling τ_p . Our results indicate also negligible effects on $E(k)$, $D(k)$, and the correlation $\langle u_1(v_1 - u_1) / \tau_p \rangle$.

3. Effects of volumetric fraction

Here, we compare two cases, C and I, where ϕ_v of the latter is double that of the former, as seen in Table V, all other properties being the same. This is achieved by simply doubling the number of particles. Figure 10 shows $E(k)$ at $T=4$ for of cases A, C, and I. It is clear from the figure, as expected, that doubling ϕ_v enhances the two-way coupling effects. The behavior of $D(k)$ and $E(t)$ (not shown) also supports this result.

B. Effects of gravity

Here, we compare three cases, C, G, and H, with identical particle properties, as seen in Table VI, but differ in the magnitude of the applied gravitational acceleration. In case C the gravity is zero, whereas in H the gravity is double that in G, as indicated by the ratio of the terminal velocity, $v_t = g\tau_p^*$, to the rms velocity of the fluid at the injection time, u_0^* , where g is the gravitational acceleration. The maximum value of v_t/u_0^* is limited in our simu-

TABLE V. Particle properties for the study of the effects of the volumetric fraction.

Case	τ_p^*	d	ρ_p/ρ	ϕ_v	ϕ_m
C	0.50	5.0×10^{-4}	1818	2.5×10^{-4}	0.45
I	0.50	5.0×10^{-4}	1818	5.0×10^{-4}	0.91

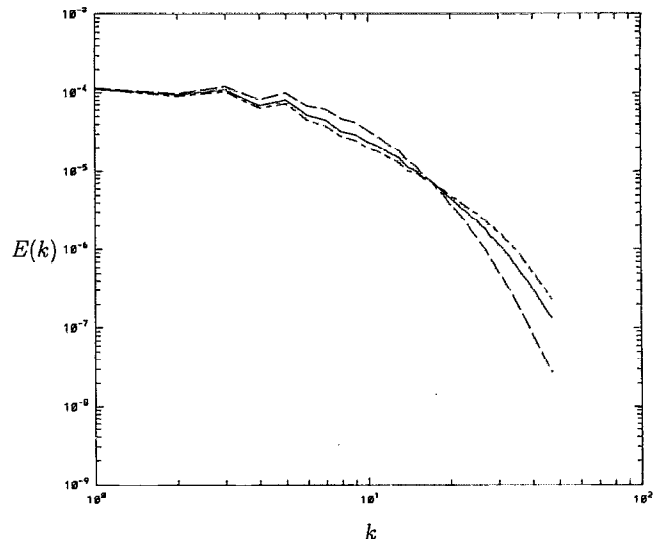


FIG. 10. Effect of varying ϕ_v (Table V) on the three-dimensional spatial spectrum of energy $E(k)$ at time $T=4$ for case A: ---, C: —, I: - · - ·.

lation because the higher it is the higher the dissipation, as will be discussed below, and thus lower R_λ . For cases G and H, R_λ decays, respectively, to 14.5 and 13 at $T=6$. Figures 11(a) and 11(b) display, respectively, the time development of $E(t)$ and $\epsilon(t)$ for cases A, C, G, and H. It is seen that, as time increases, the higher (v_t/u_0^*) the lower is the rate of decay of $E(t)$ and $\epsilon(t)$. In fact, for $T > 5$, we see that $E(t)$ for case H exceeds that of A, the particle-free case, and that as time increases the turbulence approaches a state of pseudostationarity, where there is a balance between the rate of energy addition (by the particles) and $\epsilon(t)$. In order to understand the mechanisms leading to this behavior, we examine the distributions of $E(k)$, $D(k)$, $T(k)$, $S(t)$ and other relevant properties of turbulence.

Figure 12 shows $E(k)$ at $T=6$ for cases A, C, G, and H, and Fig. 13 shows the corresponding $D(k)$. Instead of having one crossover wave number, k_c , relative to case A, as in Fig. 3 ($k_c=18$), we see in Fig. 12 that the larger the gravity the smaller is the crossover wave number. Furthermore, the crossover wave numbers of the gravity cases continue to decrease with time, whereas it remains unchanged for case C; $k_c \approx 18, 11,$ and 9 for cases C, G, and H, at $T=6$, whereas at the earlier time $T=4$, the corresponding values are $k_c \approx 18, 15,$ and 11 (not shown). Also, $D(k)$ shows a similar behavior in Fig. 13. This indicates that the energy transfer from the particles to the turbulence starts, as expected, at high wave numbers, and as these become “saturated,” the excess energy is transferred

TABLE VI. Particle properties for the study of the effects of gravity.

Case	τ_p^*	d	ρ_p/ρ	ϕ_v	ϕ_m	v_t/u_0^*
C	0.50	5.0×10^{-4}	1818	2.5×10^{-4}	0.45	0.0
G	0.50	5.0×10^{-4}	1818	2.5×10^{-4}	0.45	0.25
H	0.50	5.0×10^{-4}	1818	2.5×10^{-4}	0.45	0.50

TABLE VII. Particle properties normalized by relevant scales of turbulence.

Case	τ_p^*/τ_f	τ_p^*/τ_K	d/l^*	d/η^*	$R_{\rho,max}$
C	$0.289 \Rightarrow 0.079$	$2.252 \Rightarrow 0.764$	0.007	0.158	0.27
G	$0.289 \Rightarrow 0.088$	$2.525 \Rightarrow 0.955$	0.007	0.158	0.28
H	$0.289 \Rightarrow 0.104$	$2.525 \Rightarrow 1.242$	0.007	0.158	0.30

to lower wave numbers. In effect, a *reverse cascade* takes place involving nonlocal triads of $T(k)$, due to forcing by the particles at high wave numbers.

We study this mechanism further by examining the time development of the three components of the skewness $S(t)$ for cases A, C, G, and H in Fig. 14. The components of $S(t)$, rather than their sum, would shed more light on the transfer process since gravity acts in one direction, x_3 . The anisotropy of the three components of $S(t)$ is evident for the gravity cases G and H, whereas those for cases A and C show no significant directional sensitivity, and are

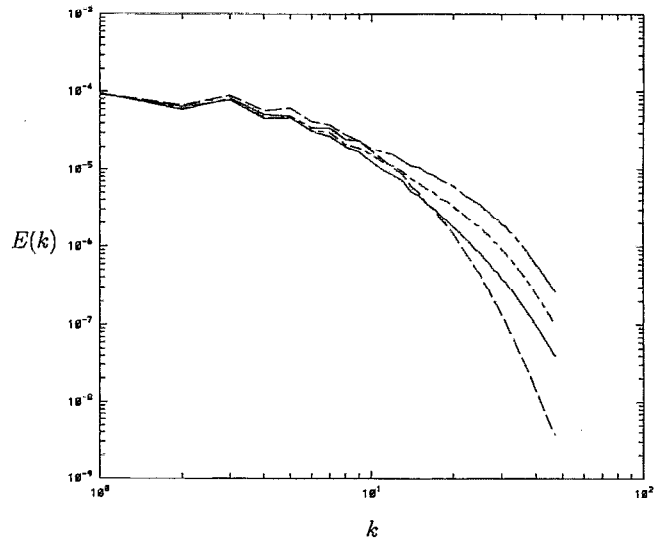
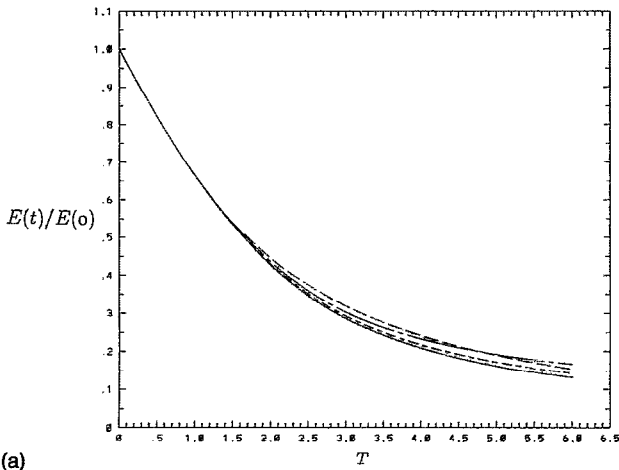


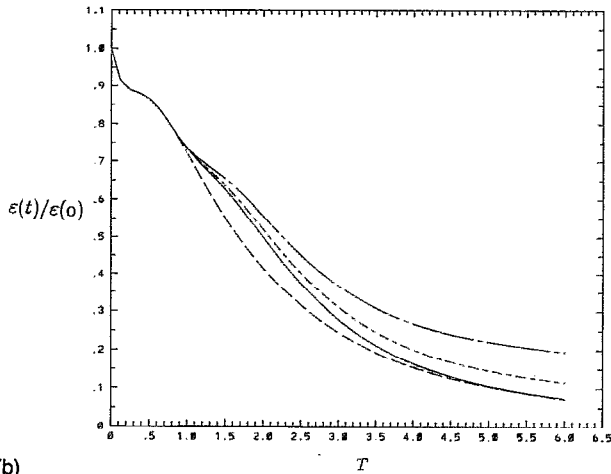
FIG. 12. Effect of varying gravitational acceleration (Table VI) on the three-dimensional spatial spectrum of energy $E(k)$ at time $T=6$ for case A: ---, C: —, G: -·-·-, H: -·-·-.

nearly time independent for $T > 1$. We see a nearly monotonic increase with time (for $T > 1.5$) of the magnitude of the components in the gravity direction for cases G and H, and a monotonic decrease of their two lateral (x_1, x_2) components. Also, the higher the gravity the larger is the anisotropy. Furthermore, it is seen that the lateral components of case H change sign at $T \approx 5.5$. Equation (14) indicates that a change of sign of $S(t)$ occurs *only* when $T(k)$ changes sign since all other quantities in this equation are always positive. This is verified next by comparing the components of $T(k)$ for cases C and H.

Figures 15 and 16 compare, at $T=4$, the spectral distributions of $T(k_1)$ and $T(k_3)$, respectively, for cases C



(a)



(b)

FIG. 11. (a) Effect of varying gravitational acceleration (Table VI) on the time development of turbulence kinetic energy $E(t)$ normalized by its initial value $E(0)$ for case A: ---, C: —, G: -·-·-, H: -·-·-. (b) Effect of varying gravitational acceleration (Table VI) on the time development of the dissipation rate of turbulence kinetic energy $\epsilon(t)$ normalized by its initial value $\epsilon(0)$ for case A: ---, C: —, G: -·-·-, H: -·-·-.

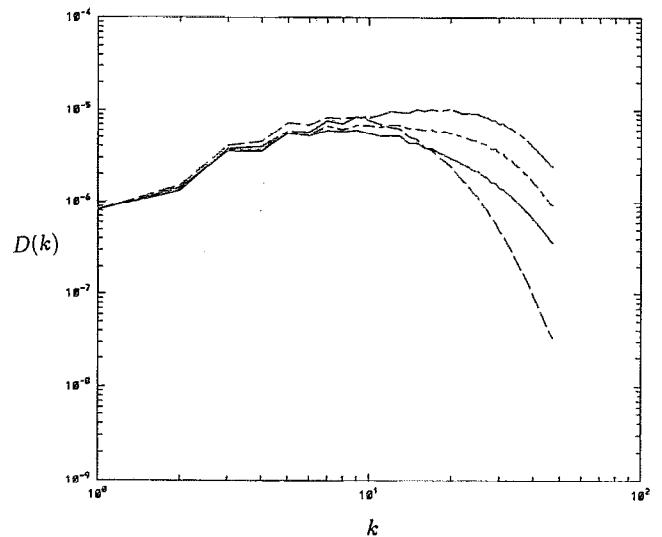


FIG. 13. Effect of varying gravitational acceleration (Table VI) on the three-dimensional spatial spectrum of energy dissipation $D(k)$ at time $T=6$ for case A: ---, C: —, G: -·-·-, H: -·-·-.

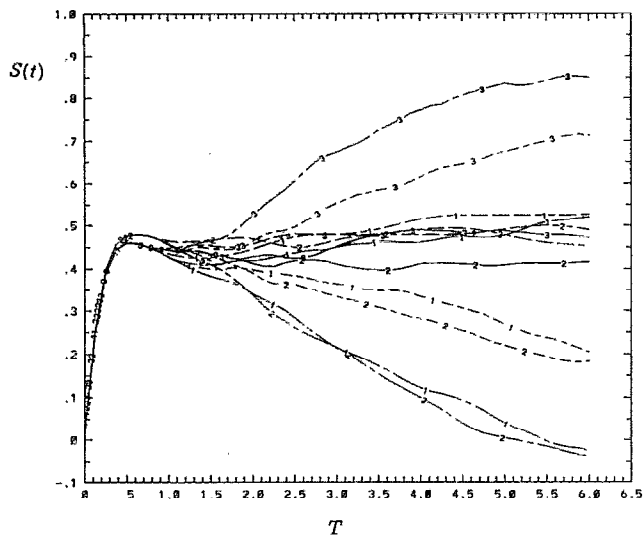


FIG. 14. Effect of varying gravitational acceleration (Table VI) on the time development of the three components (labeled 1, 2, and 3) of the skewness of the fluid velocity derivative $S(t)$ for case A: ---, C: —, G: - · - · -, H: - - -.

and H. The anisotropy of $T(k)$ in case II is evident in the higher magnitudes of $T(k_3)$ relative to those of $T(k_1)$. The augmentation of $T(k_3)$ due to gravity is seen in Fig. 16. This behavior is consistent with that of the components of $S(t)$ displayed in Fig. 14 for these two cases. The reverse cascade at $T=4$ is seen in Fig. 15 by the change of sign of $T(k_1)$ of case H at high wave numbers, as compared to the zero value for case C. This behavior persists at later times. The wave number at which $T(k_1)$ changes sign decreases with time, occurring at $(k \geq 32)$ for $T=4$, and at $(k \geq 26)$ for $T=6$. This indicates that the energy added, at high wave numbers, by the particles due to the buoyancy force in the x_3 direction, is being gradually received by lower

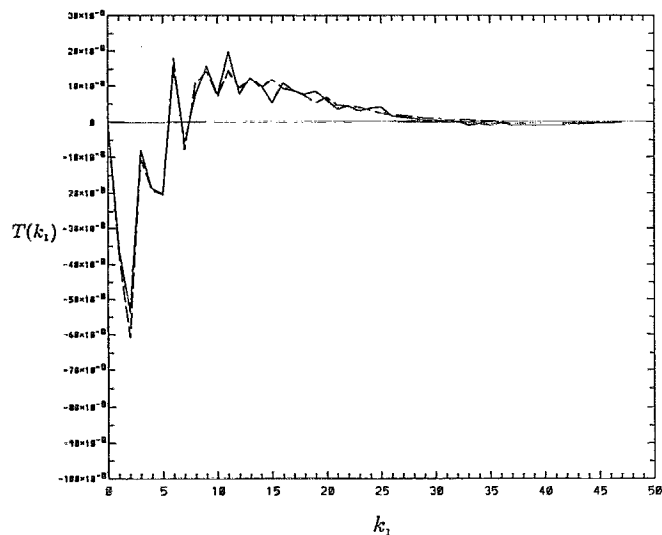


FIG. 15. Effect of varying gravitational acceleration (Table VI) on the spectral distribution of $T(k_1)$ at time $T=4$ for case C: ---, H: —.

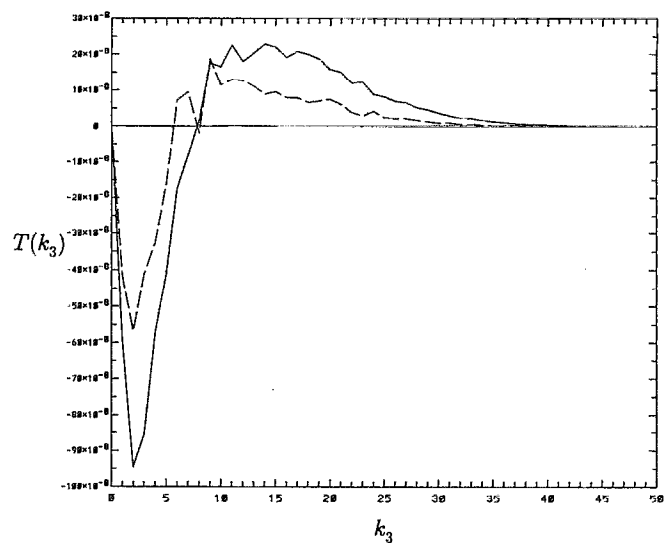


FIG. 16. Effect of varying gravitational acceleration (Table VI) on the spectral distribution of $T(k_3)$ at time $T=4$ for case C: ---, H: —.

wave numbers in the other two directions. The spectral distribution of $T(k_2)$ is quite similar to that of $T(k_1)$, and thus is not shown.

A direct measure of the anisotropy of the high wave number motion is the trace of the dissipation anisotropy tensor D_{ij} defined as

$$D_{ij} = \frac{2\nu \langle u_{i,j} u_{j,i} \rangle}{\epsilon} - \frac{1}{3} \delta_{ij}. \quad (16)$$

A measure of the anisotropy of the low wave-number motion is the trace of the energy anisotropy tensor B_{ij} defined as

$$B_{ij} = \frac{\langle u_i u_j \rangle}{2E} - \frac{1}{3} \delta_{ij}. \quad (17)$$

The time development of D_{ij} for cases A, C, G, and H (not shown) indicates that the deviation from isotropy, $D_{ii}=0$, is greatest for case H, followed by case G, whereas it is negligible for the other cases. The behavior of B_{ij} is qualitatively similar to that of D_{ij} but with smaller magnitudes. The dominant contribution of $\langle u_3^2 \rangle$, in the direction of gravity, to the energy E is always larger than the other two components, and it increases monotonically with time. Thus, the higher values of $E(t)$ in case H relative to the other cases is due only to the increase of $\langle u_3^2 \rangle$.

The role of the pressure-strain correlation $\langle pu_{i,i} \rangle$ in redistributing the energy of the x_3 direction to the other two directions is shown in Fig. 17 which displays the time development of the three components of $\langle pu_{i,i} \rangle$ for case H. It is seen that $\langle pu_{3,3} \rangle$ is always negative for $T > 1$ and its magnitude increases monotonically, indicating the continuous transfer of energy from the gravity direction to the other two. On the other hand, in case C (not shown) the three components diminish in time for $T > 2$. It should be noted that the pressure-strain correlation $\langle pu_{3,3} \rangle$ transfers energy locally, i.e., at the same wave number to the other

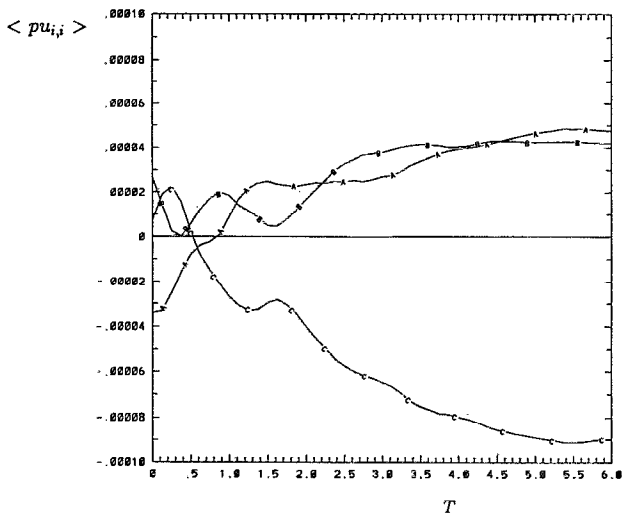


FIG. 17. Time development of the components of the pressure-strain tensor for case H (Table VI); $\langle pu_{1,1} \rangle$: A, $\langle pu_{2,2} \rangle$: B, $\langle pu_{3,3} \rangle$: C.

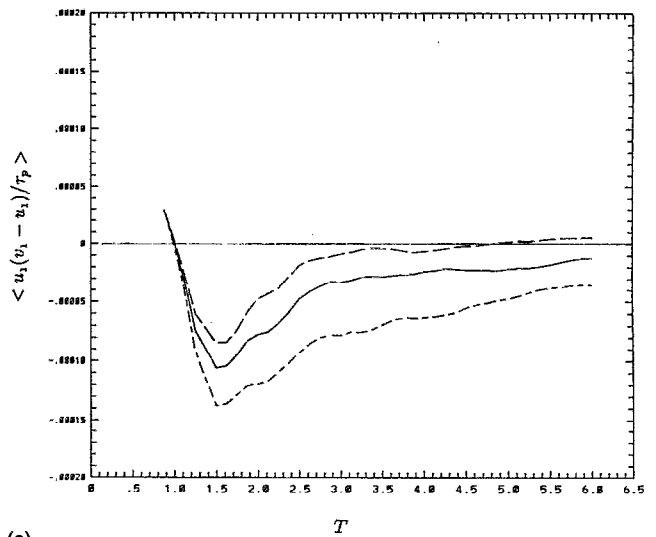
two directions x_1 and x_2 , where the energy is, otherwise, negligible. This contrasts the role of $T(k)$ which transfers energy in the same direction but to different wave numbers, according to the triadic interactions.

Finally, we show the source of the anisotropy discussed above by displaying the time development of the x_1 and x_3 components of the correlation $\langle \Phi u_i (v_i - u_i) / \tau_p \rangle$, respectively in Figs. 18(a) and 18(b) for cases C, G, and H. The x_3 component of G and H increases monotonically with time, while that of C is negative for $T < 4.5$ and vanishes thereafter. The x_1 component for G and H remains negative for $T > 1$, while that of C behaves nearly as its x_3 component due to isotropy. It is clear that the buoyancy force provides a continuous source of energy in the direction of the gravitational acceleration.

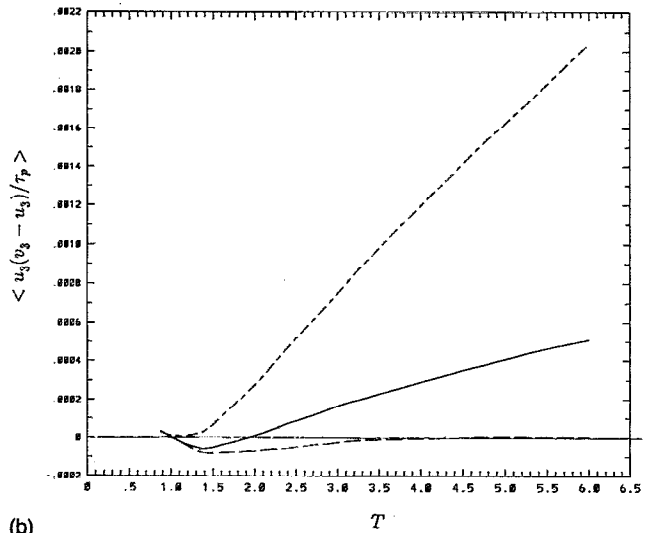
It is evident from the above discussion that the most important effect of gravity is the anisotropy of the small-scale motion (large wave numbers) of the carrier fluid, as indicated in the time behavior of the trace $D_{ii}(t)$ of the dissipation anisotropy tensor. This anisotropy is caused by the directionality of the correlation $\langle \Phi u_i (v_i - u_i) / \tau_p \rangle$ [Figs. 18(a) and 18(b)] which in turn causes the anisotropy of $\Psi_p(k_i)$. Consequently, the pressure-strain correlation $\langle pu_{3,3} \rangle$ transfers energy locally to the other two directions x_1 and x_2 , where the energy is, otherwise, negligible. Yakhot and Pelz²⁶ used direct numerical simulation of homogeneous turbulence in which anisotropic forcing was applied to the large wave-number region. They showed that small-scale anisotropy is the determining factor in the process of reverse cascading the energy to the large-scale motion.

IV. CONCLUDING REMARKS

The paper examines the turbulence modification due to the two-way interaction between decaying turbulence and



(a)



(b)

FIG. 18. (a) Effect of varying gravitational acceleration (Table VI) on the time development of the correlation $\langle u_1(v_1 - u_1) / \tau_p \rangle$ for case C: ---, G: —, H: - · - · -. (b) Effect of varying gravitational acceleration (Table VI) on the time development of the correlation $\langle u_3(v_3 - u_3) / \tau_p \rangle$ for case C: ---, G: —, H: - · - · -.

small solid particles ($d < \eta$ and $\tau_p \approx \tau_K$) dispersed within. It has been demonstrated that the particles, in the absence of gravity, transfer their momentum to the high wave-number motion of the carrier fluid, thus increasing the energy content of the small scales. This increase of energy is accompanied by an increase of the viscous dissipation rate, and, hence, an increase in the rate of energy transfer $T(k)$ from the large-scale motion. Thus, depending on the conditions at particle injection, the fluid turbulence kinetic energy may increase initially. But, in the absence of external sources (shear or buoyancy), the turbulence energy will eventually decay faster than in the particle-free turbulence. This enhanced decay of energy increases the growth rate of the integral length scale and reduces the Kolmogorov length scale.

In gravitational environment, particles also transfer

their momentum to the small-scale motion but in an *anisotropic* manner. The pressure-strain correlation acts to remove this anisotropy by transferring energy from the direction of gravity to the other two directions, *but at the same wave number*, i.e., to the small-scale motion in directions normal to gravity. This input of energy in the two directions with lowest energy content causes a *reverse cascade*. This reverse cascade tends to build up the energy level at lower wave numbers, thus reducing the decay rate of energy as compared to that of particle-free turbulence. This reduction of the energy decay rate slows down the rate of growth of the integral length scale. The associated augmentation of the dissipation rate reduces the Kolmogorov length scale.

ACKNOWLEDGMENTS

Most of the computations for this work were performed on the Cray Y-MP8/864 at the San Diego Supercomputer Center through an allocation grant. The work was also supported by the University of California—Irvine through an allocation of computer time on the Convex C240.

- ¹G. Hetsroni and M. Sokolov, "Distribution of mass, velocity and intensity of turbulence in a two-phase jet," *J. Appl. Mech.* **38**, 315 (1971).
- ²J. Popper, N. Abuaf, and G. Hetsroni, "Velocity measurements in a two-phase turbulent jet," *Int. J. Multiphase Flow* **1**, 715 (1974).
- ³D. Modarress, H. Tan, and S. Elghobashi, "Two-component LDA measurement in a two-phase turbulent jet," *AIAA J.* **22**, 624 (1984).
- ⁴D. Fleckhaus, K. Hishida, and M. Maeda, "Effect of laden solid particles on the turbulent flow structure of a round free jet," *Exp. Fluids* **5**, 323 (1987).
- ⁵Y. Tsuji, Y. Morikawa, T. Tanaka, K. Kariminc, and S. Nishida, "Measurements of an axisymmetric jet laden with coarse particles," *Int. J. Multiphase Flow* **14**, 565 (1988).
- ⁶Y. Levy and F. C. Lockwood, "Velocity measurements in a particle-laden turbulent free jet," *Combust. Flame* **40**, 333 (1981).
- ⁷Y. Hardalupas, A. M. K. P. Taylor, and J. H. Whitelaw, "Velocity and particle-flux characteristics of turbulent particle-laden jets," *Proc. R. Soc. London Ser. A* **426**, 31 (1989).
- ⁸G. Hetsroni, "Particle-turbulence interaction," *Int. J. Multiphase Flow* **15**, 735 (1989).
- ⁹R. A. Gore and C. T. Crowe, "Effect of particle size on modulating turbulent intensity," *Int. J. Multiphase Flow* **15**, 279 (1989).
- ¹⁰G. C. Truesdell and S. E. Elghobashi, "On the two-way interaction between homogeneous turbulence and dispersed solid particles. II. Effects on particle dispersion," *Phys. Fluids A* (to be submitted, 1993).
- ¹¹K. D. Squires and J. K. Eaton, "Particle response and turbulence modification in isotropic turbulence," *Phys. Fluids A* **2**, 1191 (1990).
- ¹²S. E. Elghobashi and G. C. Truesdell, "Direct simulation of particle dispersion in decaying isotropic turbulence," *J. Fluid Mech.* **242**, 655 (1992).
- ¹³T. Gerz, U. Schumann, and S. Elghobashi, "Direct simulation of stably stratified homogeneous turbulent shear flows," *J. Fluid Mech.* **200**, 563 (1989).
- ¹⁴U. Schumann, "Realizability of Reynolds-stress turbulence models," *Phys. Fluids* **20**, 721 (1977).
- ¹⁵I. Kim, S. Elghobashi, and W. Sirignano, "Three-dimensional flow over two spheres placed side by side," *J. Fluid Mech.* **246**, 465 (1993).
- ¹⁶P. K. Yeung and S. B. Pope, "An algorithm for tracking fluid particles in numerical simulations of homogeneous turbulence," *J. Comput. Phys.* **79**, 373 (1988).
- ¹⁷S. Balachandar and M. R. Maxey, "Methods for evaluating fluid velocity in spectral simulations of turbulence," *J. Comput. Phys.* **83**, 96 (1989).
- ¹⁸G. C. Truesdell, "The interaction between decaying isotropic turbulence and dispersed solid particles," Ph.D. dissertation, University of California, Irvine, 1993.
- ¹⁹G. K. Batchelor, *The Theory of Homogeneous Turbulence* (Cambridge University Press, Cambridge, 1953), p. 101.
- ²⁰J. O. Hinze, *Turbulence* (McGraw-Hill, New York, 1975), pp. 211–215.
- ²¹J. G. Brasseur and S. Corrsin, "Spectral evolution of the Navier–Stokes equations for low order couplings of Fourier modes, in *Advances in Turbulence*, edited by G. Comte-Bellot and J. Mathieu (Springer-Verlag, New York, 1987), pp. 152–162.
- ²²J. A. Domaradzki and R. S. Rogallo, "Local energy transfer and non-local interactions in homogeneous, isotropic turbulence," *Phys. Fluids A* **2**, 413 (1990).
- ²³K. Ohkitani and S. Kida, "Triad interactions in a forced turbulence," *Phys. Fluids A* **4**, 794 (1992).
- ²⁴C. W. Van Atta and W. Y. Chen, "Measurements of spectral energy transfer in grid turbulence," *J. Fluid Mech.* **38**, 743 (1969).
- ²⁵S. Tavoularis, J. C. Bennett, and S. Corrsin, "Velocity-derivative skewness in small Reynolds number, nearly isotropic turbulence," *J. Fluid Mech.* **88**, 63 (1978).
- ²⁶V. Yakhot and R. Pelz, "Large-scale structure generation by anisotropic small-scale flows," *Phys. Fluids* **30**, 1272 (1987).